Improving handheld Laser Scanning Point Cloud Quality in Forests via RTK-GNSS integrated SLAM

Carolin Rünger[1], Stefan Binapfl[2], Sophia Böhme[1], Ferdinand Maiwald[2], Anette Eltner[1]

[1] Institute of Photogrammetry and Remote Sensing, Dresden University of Technology, 01069 Dresden, Germany – (carolin.ruenger, anette.eltner)@tu-dresden.de – sophia.boehme1@mailbox.tu-dresden.de
[2] Geodetic Institute, Dresden University of Technology, 01069 Dresden, Germany – (stefan.binapfl, ferdinand.maiwald)@tu-dresden.de

Keywords: Handheld Personal Laser Scanning, Mobile Laser Scanning, RTK-GNSS Integrated SLAM, Forest Inventory, Tree Parameters, Quantitative Structure Model.

Abstract

Accurate forest inventories are essential for sustainable forest management. Handheld personal laser scanning (H-PLS) enables efficient and flexible forest data acquisition. However, ensuring reliable point cloud quality in complex environments remains challenging. While Simultaneous Localization and Mapping (SLAM)-based H-PLS allows rapid data collection, trajectory drift and accumulated registration errors can reduce the accuracy of derived tree parameters and structural metrics. In contrast, Global Navigation Satellite System (GNSS)-based Real-Time Kinematic (RTK) positioning provides centimetre-level absolute accuracy and drift-free trajectories, although its application in forested environments is still emerging. This study evaluates the impact of RTK-GNSS integration on point cloud geometry compared to SLAM-based point clouds without GNSS across two Central European forest plots with contrasting canopy structures. Analyses focused on tree parameter accuracy, structural metrics based on quantitative structural models, point density and noise characteristics. To isolate the effect of GNSS integration, data from the RTK-GNSS enabled H-PLS device were additionally processed without GNSS information, and an open-trajectory scan without loop closure was included for comparison. Results show that RTK-GNSS improves point cloud consistency and especially enhances the estimation of volume- and branch-related metrics. In the dense canopy plot, RTK-GNSS information reduced mean errors in branch number (−6100 to −5369) and crown volume (−492.75 to −357.21 m³). However, overall performance in tree parameter estimation depends on point density. These findings highlight RTK-GNSS H-PLS as a promising approach for flexible and efficient forest data acquisition in inventory applications.

1. Introduction

In recent years, handheld personal laser scanners (H-PLS) have emerged as flexible systems for capturing three-dimensional (3D) data across various environments, including complex natural scenes where traditional static scanning is impractical. In forestry, they are used to derive tree parameters such as diameter at breast height (DBH), tree height and other structural attributes (Kuželka et al., 2022; Chudá et al., 2024). H-PLS typically rely on Simultaneous Localization and Mapping (SLAM), combining LiDAR and inertial measurement unit (IMU) data to reconstruct 3D point clouds while simultaneously estimating the sensor trajectory.

However, SLAM is based on relative measurements, which leads to accumulated errors and trajectory drift. In forests, similar tree structures and vegetation dynamics can further challenge mapping, resulting in duplicated stems and distorted point clouds that reduce the accuracy of derived tree parameters (Qian et al., 2017). In contrast, Global Navigation Satellite System (GNSS)-based Real-Time Kinematic (RTK) positioning provides centimetre-level absolute accuracy and drift-free trajectories, but signal obstruction in dense forests can degrade positioning quality (Pirti et al., 2010). Combining RTK and SLAM improves system robustness by compensating for individual limitations and enhances the operational reliability of H-PLS. Moreover, RTK-GNSS enables direct global georeferencing without ground control points (GCPs) and supports open trajectories.

Despite the potential of hybrid systems, most H-PLS devices still lack integrated RTK capability, which limits their ability to achieve absolute positioning. A promising step toward closing this gap is represented by a H-PLS that integrates RTK-GNSS, IMU, LiDAR and camera measurements in SLAM, allowing for relative and absolute positioning. When the scanner reaches an area with weak or no GNSS signal, it uses its LiDAR, IMU and camera data to inversely calculate the current RTK point coordinates. When signal is available again RTK information is used to re-initialize and correct the position (Shanghai Huace Navigation Technology Ltd., 2025).

Integrating RTK-GNSS in SLAM is expected to improve point cloud quality by enhancing geometric accuracy and spatial consistency, as RTK continuously corrects the trajectory and prevents drift-related distortions. This should reduce noise and improve the internal geometry of point clouds, resulting in more reliable representation of forest structures for more accurate extraction of tree attributes. Therefore, this study aims to evaluate whether RTK-GNSS integration leads to improvements in point cloud geometry compared to SLAM operating without GNSS, with a particular focus on tree attributes.

Specifically, we conducted tree instance segmentation to separate individual trees from the point cloud, derived classical tree parameters such as DBH and performed full 3D tree reconstruction using quantitative structural models (QSM) to capture detailed structure and branching architecture. In addition, point density and noise characteristics were evaluated. All analyses systematically compared RTK-GNSS SLAM H-PLS with SLAM without GNSS point clouds. To isolate the specific influence of GNSS integration, RTK-GNSS data were additionally processed without GNSS information, and an additional scan was acquired using an open trajectory without loop closure.

https://doi.org/10.5194/isprs-archives-XLIX-B2-2026-261-2026

2. Materials and Methods

2.1 Study Areas

The study was conducted in Tharandt Forest, Saxony, Germany, using two plots representing dense and sparse canopy conditions (Figure 1). The dense plot was a homogeneous Douglas-fir stand (~30 × 40 m, 1042 m²) with widely spaced trees and crowns starting high (mean height 29.4 m, DBH 0.47 m). The sparse plot was a heterogeneous stand dominated by oak with beech and ash (~20 × 40 m, 721 m²), featuring closer tree spacing and lower, more complex branching (mean height 17.9 m, DBH 0.30 m). The plots were selected to capture structural differences and to assess the RTK-GNSS integrated H-PLS performance, with stable RTK conditions expected in the sparse plot and signal limitations in the dense plot.

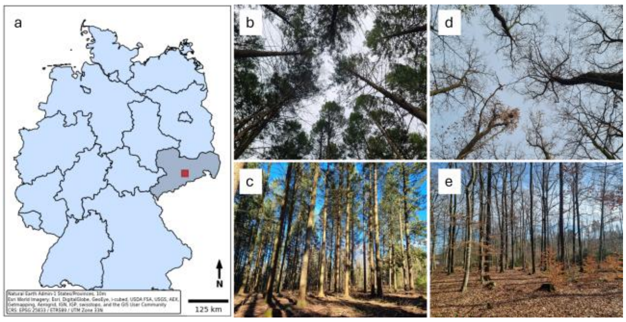

Figure 1. Study area in Tharandt Forest, Germany: (a) location within Germany (red rectangle); (b) canopy cover of the dense canopy plot; (c) trees in the dense canopy plot; (d) canopy cover of the sparse canopy plot; (e) trees in the sparse canopy plot.

2.2 H-PLS Data and Reference Data Collection

H-PLS data were acquired in January 2026 under leaf-off conditions, which improve visibility of structural features, using three scanners: CHCNav RS10 (RS10), GeoSLAM ZEB-Horizon (ZEB) and Leica BLK2GO (BLK). The technical specifications can be found in Table 1. The systems differ in their SLAM approaches: RS10 integrates RTK-GNSS, IMU, LiDAR, and camera data for georeferenced positioning in real time, ZEB uses LiDAR-IMU SLAM and BLK combines LiDAR, camera, and IMU data in a SLAM framework.

Technical specification	RS10	ZEB	BLK
Range	120 m	100 m	25 m
Field of view (H,V)	360°, 270°	360°, 270°	360°, 270°
Channel	16	16	n/a
Scan rate (pts/s)	320.000	300.000	420.000
Relative position accuracy	< 1 cm	< 6 mm	6-15 mm
Absolute position accuracy (H, V)	< 5 cm RMSE	n/a	n/a
RTK-GNSS	Yes	No	No
Number of cameras	3	0	4
Operating temperature	-20-50 °C	0-50°C	0-40 °C

Table 1. Technical specifications of the H-PLS.

All scanners were operated along a looped trajectory at ~1 m/s for about 8 minutes per plot (Figure 2), with RS10 additionally providing GNSS signal quality. To assess RTK-GNSS effects, RS10 data were processed with and without RTK and also acquired along an open trajectory with RTK (~4 minutes). The other systems relied on loop closure, which is essential for SLAM in forest environments (Tsintotas et al., 2022). A high-resolution TLS reference point cloud was collected using a RIEGL VZ-400i from 17 scan positions per plot, and manual DBH measurements were taken for 10 trees per plot with a tree caliper.

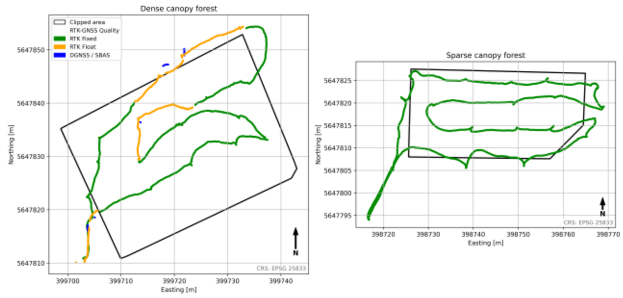

Figure 2. Acquisition trajectory for the H-PLS surveys in the plots, including the walking path, the cropped area used in this study and the RTK-GNSS signal quality of the RS10.

2.3 Point Cloud Pre-Processing and Tree Segmentation

Point clouds were pre-processed using the respective software (RS10: CoPre2, ZEB: GeoSLAM Connect Viewer, BLK: Leica Register 360 Plus, TLS: RiSCAN PRO). All H-PLS data were co-registered to TLS using manual alignment followed by ICP and then cropped to identical extents (Figure 2), resulting in 25 trees (dense) and 40 trees (sparse).

Tree instance segmentation was performed automatically using TreeLearn (Henrich et al., 2024) with default parameters. TreeLearn is a deep learning-based method trained on manually segmented forest point clouds that first classifies points as tree or non-tree and predicts offsets toward the tree base. These offset-corrected points are then clustered to identify individual trees, followed by postprocessing to refine the segmentation. False segmented points were reduced using connected component analysis by retaining only the largest component per tree. To preserve the crown points, less filtering applied in the upper canopy. Final segmentation is shown in Figure 3.

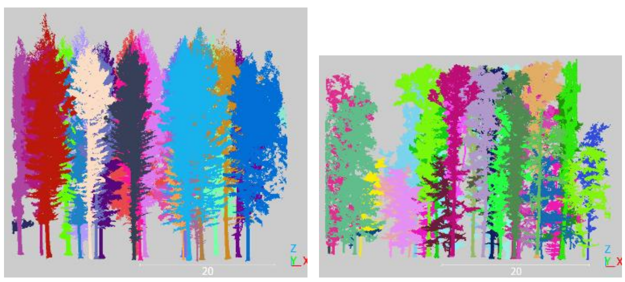

Figure 3. TLS single-tree segmentation after connected component analysis in dense (left) and sparse (right) canopy forest; colours indicate tree IDs.

2.4 Determination of Tree Parameters

Tree parameters were automatically extracted using ITSMe v2.0.0 (Terryn, 2025), an R-based tool for individual tree analysis. The parameters enable a comprehensive assessment of measurement accuracy in mobile laser scanning based forest inventories (Table 2).

Tree height reflects the ability to capture vertical structure and treetop detection, DBH indicates tree growth and productivity, and functional DBH (fDBH) accounts for irregular stem shapes. Horizontal tree-to-tree distances were calculated from XY coordinates as Euclidean distances (190 pairs in the dense plot, 300 in the sparse) to assess internal point cloud geometry. All values were computed within the cropped area and compared to the TLS reference.

Tree parameter	Unit	Description
XY Position	m	Mean coordinates of the 100 lowest points
Height	m	Difference between maximum and minimum Z-values
Diameter at breast height (DBH)	m	Horizontal slice at 1.3 m, circle fit to points
Functional DBH (fDBH)	m	Horizontal slice at 1.3 m, convex hull-based diameter

Table 2. Tree parameters calculated using ITSMe.

2.5 Quantitative Structure Model

For four representative trees located in the centre of each plot, QSMs were generated using TreeQSM v2.4.1 (Raumonen and Åkerblom, 2022). The models represent trees as connected cylinders, from which structural parameters were extracted and compared to TLS (Table 3). QSM was chosen because it detects more branches and provides richer structural metrics than density-based clustering approaches (Winberg et al., 2023). Branching metrics assess the reconstruction of tree architecture, crown metrics capture upper-tree geometry and spatial extent, and volume metrics evaluate biomass, wood volume, and overall reconstruction accuracy. Together, these represent structural complexity from fine-scale features to whole-tree properties.

	Tree metrics	Unit	Description
Branching	Branch Length	m	Sum of the lengths of all cylinders forming a branch
	Number of Branches	-	The total number of branch IDs in the QSM model
	Max Branch Order	-	Largest branch order
Crown	Crown Base Height	m	Height of the lowest branch of the crown above the ground
	Crown Diameter	m	Mean horizontal diameter of the crown
	Crown Area	m^2	Horizontal crown area calculated from an alpha shape of the crown points
Volume	Branch Volume	m^3	Sum of the volumes of all cylinders of a branch
	Crown Volume	m^3	Crown volume calculated using a 3D alpha shape
	Trunk Volume	m^3	Sum of all cylinders assigned to the trunk
	Total Volume	m^3	Sum of all cylinders in the QSM model

Table 3. Tree metrics calculated using TreeQSM.

2.6 Noise und Point Density

For all trees in the cropped areas, horizontal and vertical point cloud characteristics were analysed. Horizontal noise at DBH level was measured from a 20 cm stem slice at 1.3 m as mean absolute distance to a fitted circle and ring thickness, calculated as the average difference between the maximum and minimum radius of the points within each 10° angular segment. Branch-level point densities were compared across H-PLS and to TLS. Vertical distribution of the points was assessed by slicing trees into 20 cm layers every 50 cm along the stem, calculating point density per cubic meter, and summarizing overall densities per scanner.

2.7 Statistical Analysis

To assess tree parameter accuracy, scanner measurements x_i were compared to TLS references values $\hat{x}_i$ to quantify deviations between the two datasets. Mean error (ME) and root mean square error (RMSE) were calculated to capture systematic bias and overall magnitude of errors, with values expressed in the same units as the respective parameter.

$$ME = \frac{1}{N}\sum_{i=1}^{N}(x_i - \hat{x}_i)\,;\, RMSE = \sqrt{\frac{1}{N}\sum_{i=1}^{N}(x_i - \hat{x}_i)} \quad (1)$$

Agreement was further evaluated using the Concordance Correlation Coefficient (CCC), which ranges from −1 (perfect negative agreement) to 1 (perfect agreement) and quantifies how closely the observations align with the 1:1 line.

$$CCC = \frac{2 \times cov(x_i, \hat{x}_i)}{var(x_i) + var(\hat{x}_i) + (\bar{x}_i - \bar{\hat{x}}_i)^2} \quad (2)$$

3. Results

3.1 Point Cloud Density and Noise

At DBH level, horizontal noise was lowest for RS10 and BLK, both closely matching TLS (ME ≈ 0.001–0.002 m), while ZEB showed higher noise (up to ~0.009 m). For ring thickness, RS10 consistently produced smaller values than TLS (ME ≈ −0.02 to −0.03 m), whereas BLK results were similar to TLS. In contrast, ZEB showed the largest deviations, especially in the sparse plot (ME ~0.14 m, RMSE ~0.36 m) (Figure 4).

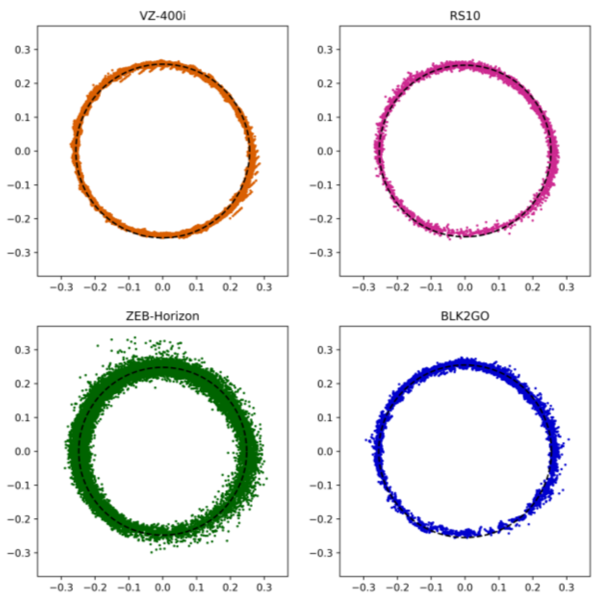

Figure 4. Horizontal noise at DBH level (20 cm cross-section) of a stem, shown for a representative tree in the dense canopy forest.

Vertical point density profiles clearly differed between scanners (Figure 5). ZEB showed the highest densities, including in the canopy, while RS10 was considerably sparser. BLK provided slightly higher densities than RS10 but was limited to ~20 m height due to its 25 m range. These differences are also clearly visible in Figure 6, which shows the same tree scanned with all devices.

https://doi.org/10.5194/isprs-archives-XLIX-B2-2026-261-2026

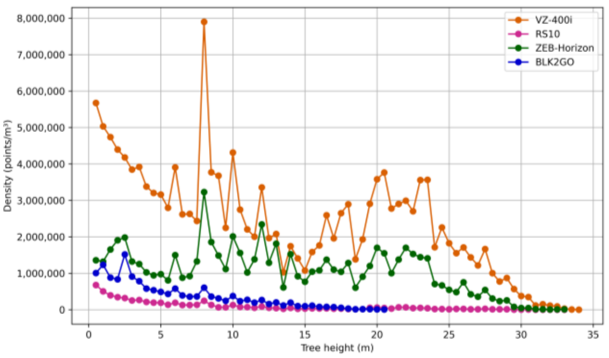

Figure 5. Vertical point density profile of a representative tree in the dense canopy forest.

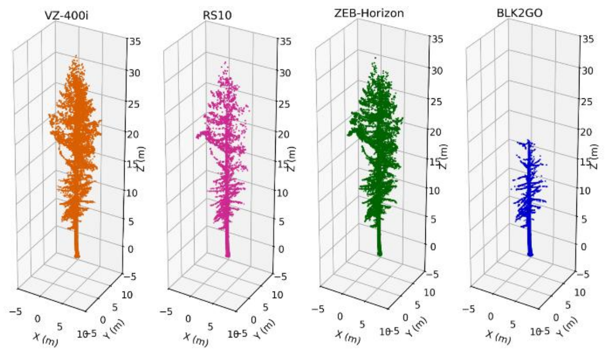

Figure 6. Comparison of the point cloud for the same tree in the dense canopy forest.

Overall, ZEB produced the densest point clouds, RS10 the sparsest, and BLK intermediate densities (Table 4). This is also evident in the branch-level point densities (Figure 7). ZEB again shows noticeable point noise, while RS10 exhibits low point density. BLK, in contrast, represents the branches very accurately. TLS also shows considerable noise, possibly due to wind effects.

Plot	TLS	RS10	ZEB	BLK
1	3070.19	158.92	836.02	635.11
2	7340.21	481.17	2192.07	1171.83

Table 4. Overall point density (pts/m³) for dense (Plot 1) and sparse canopy forest (Plot 2).

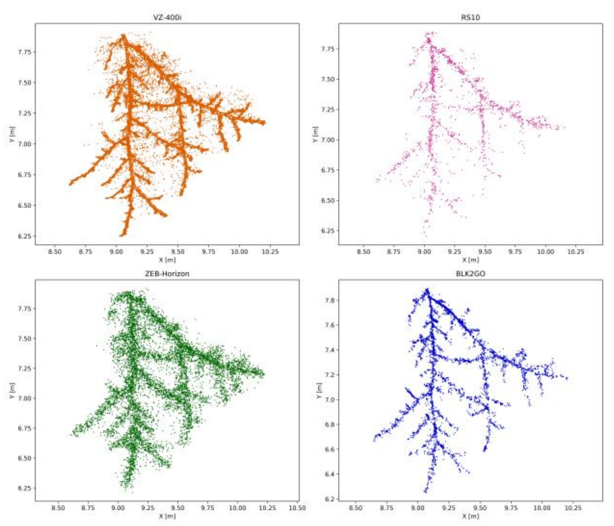

Figure 7. Branch-level point densities for a representative lower branch in the sparse canopy forest.

3.2 Tree Parameters and Position Accuracy

The comparison of tree parameter across H-PLS systems and canopy conditions is illustrated in Figure 8.

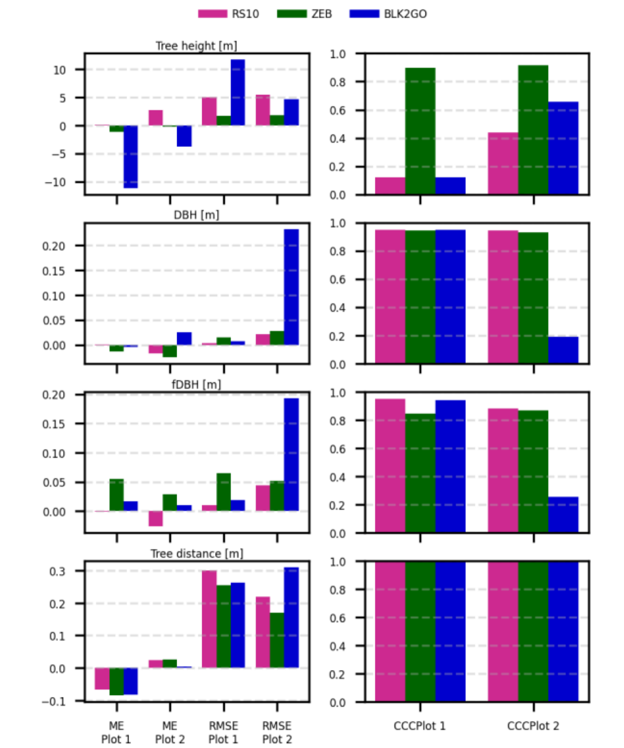

Figure 8. Comparison of tree parameters from H-PLS scanners in dense (Plot 1) and sparse canopy conditions (Plot 2).

Height: RS10 showed low bias in the dense plot (ME = 0.03 m) but high variability (RMSE ≈ 4.9–5.5 m), indicating accurate mean heights but large deviations for individual trees, resulting in low CCC. ZEB maintained low errors (ME ≈ −1.18 to −0.22 m; RMSE ≈ 1.62–1.85 m) and high agreement (CCC > 0.9), confirming its suitability for height estimation. BLK strongly underestimated tree height, especially in the dense plot (ME = −11.15 m), due to its limited 25 m range, with low CCC (0.12) in dense and moderate (0.66) in sparse conditions.

DBH: All scanners showed low ME, with RS10 having the smallest errors (0.0002 m and −0.02 m). RMSE was lowest for RS10 in both plots (0.004 m and 0.02 m) and for BLK in the dense plot (0.007 m), while BLK increased in the sparse plot (0.23 m). ZEB showed higher RMSE in the dense plot (0.015 m) but was similar to RS10 in the sparse plot (0.03 m). Concordance was high for RS10 in both plots and for ZEB and BLK in the dense plot (CCC ≈ 0.95), whereas BLK showed poor agreement in the sparse plot (CCC = 0.19). Results are in line with the manually measured DBH (Table 5).

	ME (cm)		RMSE (cm)	
Plot	1	2	1	2
TLS	-0.72	-0.35	1.86	0.91
RS10	-0.6	-1.73	1.31	1.94
ZEB	-1.93	-2.22	2.23	2.41
BLK	-0.89	-2.13	1.64	2.46

Table 5. Mean error (ME) and root mean square error (RMSE) values for manually measured DBH, for dense (Plot 1) and sparse canopy forest (Plot 2).

fDBH: RS10 showed minimal errors, especially in the dense plot, where the ME was −0.001 m and the RMSE was 0.01 m, indicating very close agreement with TLS and resulting in high concordance with a CCC of 0.95. It also remained reliable in the sparse plot with a CCC of 0.88. ZEB slightly overestimated fDBH in the dense plot with a ME of 0.05 m but improved in the sparse plot with a reduced ME of 0.03 m, while maintaining relatively stable agreement with CCC values between 0.85 and 0.87. BLK performed well in the dense plot with a low RMSE of 0.02 m, but showed strong deviations in the sparse plot, where the RMSE increased to 0.19 m and the CCC dropped to 0.25.

Tree distances: All scanners showed only minimal systematic bias in horizontal distances between trees, with ME ranging from approximately −0.08 m to 0.03 m. However, the RMSE values revealed noticeable deviations for individual tree pairs, reaching up to about 30 cm, for example with RS10 showing an RMSE of 0.30 m in the dense plot and BLK2GO reaching 0.31 m in the sparse plot. Despite these deviations, CCC remained very high, ranging between 0.99 and 1.0, confirming that the overall relative spatial position of trees and the general stand geometry were well preserved across all point clouds.

3.3 Quantitative Structure Model Metrics

Branching: RS10 and BLK strongly underestimated branch lengths and number of branches in both plots, with very low agreement to TLS reflected by CCC values between approximately 0 and 0.15 (Figure 9). In the dense canopy, RS10 lost about 2269 m of branch length, while BLK lost approximately 2340 m. ZEB performed better overall, with moderate underestimation of branch lengths, showing ME of −823 m in the dense plot and −217 m in the sparse plot, and achieving higher concordance values between approximately 0.53 and 0.6. Maximum branch order followed the same trend across all scanners.

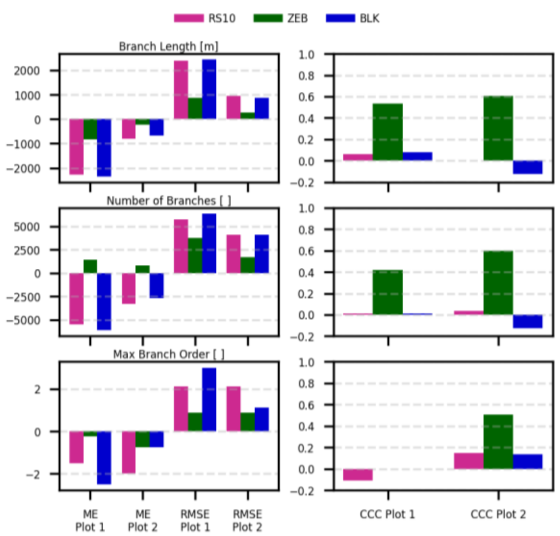

Figure 9. Comparison of branching QSM metrics from H-PLS scanners in dense (Plot 1) and sparse canopy conditions (Plot 2).

Crown: All scanners captured crown base height well (CCC ≈ 0.7–0.75) (Figure 10). RS10 excelled in the dense plot (RMSE = 0.1 m) but error increased in the sparse plot (0.47 m), while ZEB remained consistent (RMSE ≈ 0.3 m). BLK struggled in the sparse canopy (ME = -0.64 m). RS10 and BLK generally underestimated crown diameter and area, whereas ZEB was most accurate (CCC ≈ 0.7–0.74). In the sparse plot, ZEB’s RMSE were 0.57 m and 4.58 m² for diameter and area, respectively, compared to higher RMSEs for RS10 (1.13 m, 11.26 m²) and BLK (1.7 m, 14.72 m²).

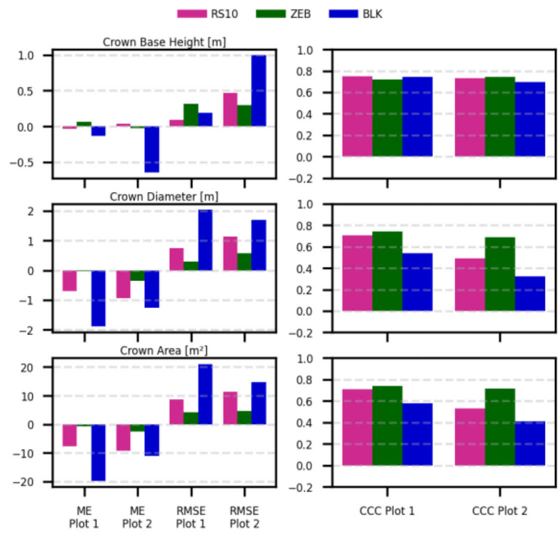

Figure 10. Comparison of crown QSM metrics from H-PLS scanners in dense (Plot 1) and sparse canopy conditions (Plot 2).

Volume: Branch volume was challenging for RS10 and BLK, especially in the dense plot, with large errors and low CCC (0.07–0.14), while ZEB outperformed them (CCC ≈ 0.6) (Figure 11). Crown and total tree volumes showed the same pattern: ZEB had low errors and high concordance, RS10 moderate performance, and BLK substantial underestimation. All scanners captured trunk volumes reliably (CCC ≈ 0.6–0.74), with RS10 best (RMSE = 449.6 m³ dense, 116.5 m³ sparse), followed by ZEB (579.3 m³, 197.1 m³) and BLK with largest deviations (816.2 m³, 247.0 m³).

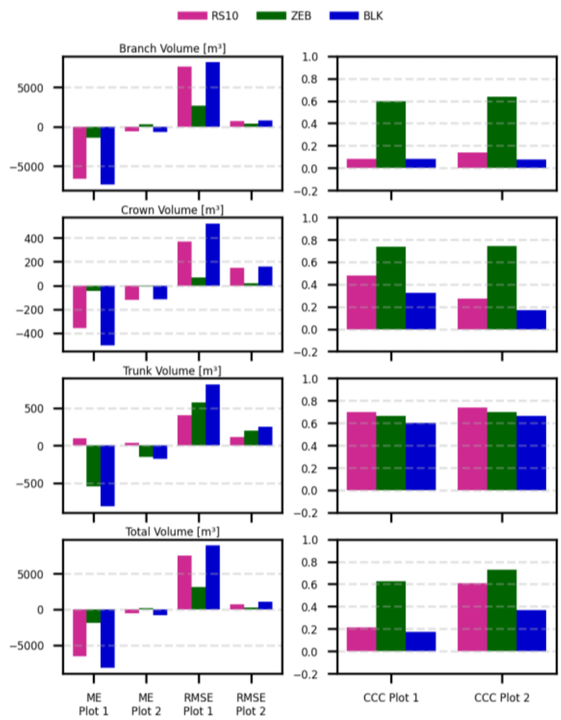

Figure 11. Comparison of volume QSM metrics from H-PLS scanners in dense (Plot 1) and sparse canopy conditions (Plot 2).

3.4 SLAM with or without RTK-GNSS and open versus closed Trajectory

Previously, we analysed scans from the RTK-GNSS SLAM H-PLS acquired using a looped trajectory with RTK-GNSS enabled. Additional scans were conducted using a looped trajectory without RTK-GNSS, where SLAM relied on LiDAR, IMU and camera data (hereafter SLAM) only. And we captured another dataset walking an open trajectory and having the RTK-GNSS enabled. This allowed comparison of tree and QSM metrics between RTK-GNSS SLAM and SLAM, as well as between open and looped trajectories. Errors relative to TLS were again calculated and averaged.

The comparison between RTK-GNSS SLAM and SLAM resulted in RTK-GNSS SLAM generally showing smaller deviations from TLS than SLAM (Table 6), especially in the dense canopy (Plot 1). This improvement is most evident for volume and branch-related metrics, which can be attributed to the higher point density of the RTK-GNSS SLAM point clouds, enabling more accurate volume estimation and a more detailed reconstruction of branches in QSM. For example, in the dense canopy, RTK-GNSS SLAM achieved a higher point cloud density of 163.55 pts/m³ compared to 158.19 pts/m³ for SLAM. In the sparse canopy (Plot 2), differences between both approaches were less pronounced. While certain metrics such as tree height and branch volume still benefited from SLAM, most of the parameters, especially branching and crown-related parameters, were more accurately captured by RTK-GNSS SLAM. Stem-related parameters (DBH, fDBH) showed only minimal differences between the two methods in both plots.

Parameter	Plot 1		Plot 2	
	RTK-GNSS	SLAM	RTK-GNSS	SLAM
Height (m)	**0.03**	-8.22	2.71	**2.23**
DBH (m)	0.0003	**0.0002**	-0.02	-0.02
fDBH (m)	**-0.0008**	0.001	-0.03	-0.03
Tree distance (m)	-0.07	-0.07	0.025	**0.005**
Branch Length (m)	**-2239.22**	-2441.89	**-822.23**	-888.99
Number Branches	**-5369**	-6100.25	**-3278**	-3473.5
Max Branch Order	**-1.75**	-3.5	**-2.75**	-3.0
Crown Base Height (m)	0.16	**0.05**	**-0.24**	-1.07
Crown Diameter (m)	**-0.65**	-2.7	**-0.88**	-2.73
Crown Area (m²)	**-8.18**	-23.65	**-9.12**	-21.51
Branch Volume (m³)	**-6709.43**	-7038.83	-607.83	**-554.73**
Crown Volume (m³)	**-357.21**	-492.75	**-118.02**	-160.72
Trunk Volume (m³)	**-87.75**	-439.75	**15.6**	208.76
Total Volume (m³)	**-6796.75**	-7478.25	-592.05	**-345.58**

Table 6. ME between RTK-GNSS SLAM and SLAM compared to TLS reference, for tree parameters and QSM metrics in dense (Plot 1) and sparse canopy forests (Plot 2). Bold values indicate better performance (lower ME).

Comparing open and looped trajectories (with RTK-GNSS enabled), the results indicated that the looped trajectory generally produced smaller deviations from TLS than the open one (Table 7), particularly in dense canopy (Plot 1). In this plot all parameters benefited from the loop closure. This improvement is caused again due to the higher point density of the looped trajectory. In the dense canopy, the looped trajectory achieved a point density of 191.18 pts/m³ compared to 114.22 pts/m³ for the open trajectory. In the sparse canopy (Plot 2), the looped trajectory also outperformed the open trajectory for nearly all parameters, with only DBH and tree distance showing slightly better results for the open trajectory. Interestingly, total volume was notably more accurate when derived from the open trajectory. The fDBH can be calculated equally well from both approaches.

Parameter	Plot 1		Plot 2	
	Open	Looped	Open	Looped
Height (m)	-1.51	**0.03**	-4.5	**2.71**
DBH (m)	-0.004	**0.0003**	**-0.004**	-0.017
fDBH (m)	-0.008	**-0.0008**	-0.03	-0.03
Tree distance (m)	-0.12	**-0.07**	**0.005**	0.02
Branch Length (m)	-2497	**-2234.3**	-975.85	**-828.35**
Number Branches	-6089.5	**-5325.5**	-3884.5	**-3313.5**
Max Branch Order	-3.0	**-2.0**	-2.75	**-2.5**
Crown Base Height (m)	1.06	**0.21**	0.06	**0.05**
Crown Diameter (m)	-2.07	**-0.81**	-3.22	**-0.93**
Crown Area (m²)	-24.25	**-9.13**	-24.45	**-9.41**
Branch Volume (m³)	-7190.4	**-6940.1**	-753.96	**-603.35**
Crown Volume (m³)	-604.84	**-363.82**	-206.59	**-120.5**
Trunk Volume (m³)	-159.25	**53.0**	558.84	**38.68**
Total Volume (m³)	-7349.8	**-6887.0**	**-194.7**	-564.48

Table 7. ME between open and looped trajectory compared to TLS reference, for tree parameters and QSM metrics in dense (Plot 1) and sparse canopy forests (Plot 2). Bold values indicate better performance (lower ME).

4. Discussion

Across all parameters, clear patterns explain scanner performance. ZEB generally performs best for structurally complex metrics such as height, branching, crown, and volume, because of its higher canopy point density, which is crucial for QSM reconstruction of fine branches and upper-crown structures. In our study, ZEB slightly overestimated fDBH due to point cloud noise. Reported DBH errors align with previous studies about ZEB (Chen et al., 2019; Gollob et al., 2020). For volume, ZEB outperformed comparable studies (e.g. Vandendaele et al. (2022): crown volume RMSE ≈ 71 m³). Tree height RMSE (1.6–1.9 m) also surpassed previous reports of RMSE ~3.4 m, but for trees heights of ~50 m (Solares-Canal et al., 2023). Unlike earlier claims that handheld PLS underestimates trees >25 m height (Hyyppä et al., 2020), ZEB and RS10 did not show this trend. Higher errors in the sparse plot indicate that stand density and occlusion, rather than tree height, primarily affect treetop detection.

RS10 performs best for stem-related parameters (DBH, fDBH, crown base height, trunk volume) and provides accurate mean tree heights, though with some outliers (RMSE 4.9–5.5 m). Positive height outliers result from the applied filtering, where false positives in the crown remain, particularly affecting smaller trees overlapped by larger ones and leading to inclusion of neighbouring tree points. Negative outliers are mainly caused by occlusion. In the sparse plot, DBH is slightly underestimated (ME ≈ -2 cm), in some cases yielding more accurate results than TLS due to the low point noise of RS10. This indicates that lower point density in stem region (Figure 5) does not necessarily reduce representation accuracy, as it strongly depends on sensor characteristics (e.g., beam divergence). Consequently, lower-density scanners can still outperform higher-density ones. However, reduced point density in the upper crown limits crown and especially branching metrics, as it hinders reliable QSM cylinder fitting. This limitation persists despite RS10’s higher scan rate and identical field of view, indicating that scan rate is not a direct indicator of data quality. Point density is also strongly influenced by processing in the scanner software. Similar effects have been reported previously, with small branches and upper-crown structures often being missed or inaccurately reconstructed (Winberg et al., 2023). Nonetheless, crown parameters remain relatively robust, suggesting that lower canopy sampling is sufficient for estimating crown geometry.

A larger ring thickness and increased point cloud noise, like observed for ZEB, can be generally explained by factors such as laser beam diameter (Abegg et al., 2021), incidence angle of the laser beam (Soudarissanane et al., 2011) and hardware and environmental influences (Feng et al., 2024). The ZEB (Velodyne VLP-16 sensor) features a horizontal beam width of 12.7 mm and divergence of 3 mrad (Muhojoki et al., 2024), whereas no explicit specifications are available for the RS10. However, its reported point cloud thickness is below 2 cm. This could indicate a smaller effective beam size and thus sharper stem representation. The lower noise in RS10 is not due to RTK-GNSS, as similar point cloud quality is observed without GNSS processing.

BLK consistently showed the lowest overall performance, mainly due to its limited scan range (25 m), which restricts the capture of upper canopy structures and branch details. This leads to systematic underestimation of tree height, confirming that insufficient sensor range reduces treetop detection (Cabo et al., 2018), and negatively affects volume estimates. However, parameters within the effective scan range are captured well. For example, BLK performed well for DBH in the dense plot (DBH ~0.7 cm; fDBH ~2 cm) but showed large deviations in the sparse plot (DBH ~23 cm; fDBH ~19 cm), indicating low robustness under more complex conditions. This is due to segmentation errors in smaller trees with low-branching, where the lower stem was segmented as a separate tree segment. As a result, DBH and fDBH were calculated without the actual stem, instead using branch and leaf points, leading to strong overestimation.

Tree-to-tree distances indicate that all scanners preserve stand geometry well, but with deviations up to ~30 cm (RS10 in dense, BLK in sparse plots). In general, the outliers align closely with the TLS reference. However, segmentation errors, as described before, affect also the accuracy of tree position. If the trunk is missing from the tree segment, the position is calculated without the actual stem and this leads to a shifted centre point and thus inaccurate tree positions. Nevertheless, ZEB was most reliable (RMSE 0.17–0.25 m). High CCC of tree distances indicates good relative positional accuracy (Muhojoki et al., 2024), making these point clouds suitable for stand structure analysis. Although these results represent relative rather than absolute accuracy, they are in a similar order of magnitude to reported absolute tree position accuracies, such as an RMSE of ~0.26 m (Chen et al., 2019) and below 0.4 m (Yang et al., 2024).

The choice of SLAM approach has a clear impact on point cloud accuracy, with RTK-GNSS SLAM outperforming SLAM without RTK-GNSS. This is particularly advantageous in forestry applications, as it provides absolute positioning without the need for ground control points, thereby enabling seamless GIS integration, precise tree localization, and easier combination with remote sensing data. The horizontal tree-to-tree distances obtained (RS10 RMSE ≈ 0.22-0.3 m) align with results from single-baseline RTK measurements in conifer stands (Cho et al., 2024). The higher point density observed with RTK-GNSS SLAM compared to SLAM without RTK can be explained by the integration of RTK-GNSS measurements into SLAM. RTK-GNSS provides absolute positioning constraints that reduce cumulative drift in the estimated scanner trajectory, leading to more consistent alignment of successive LiDAR scans and thus a denser and more accurate point cloud.

The trajectory strategy significantly affects scanner performance, with looped trajectories outperforming open ones, especially under dense canopy. This is mainly due to higher point density, as revisiting areas allows overlapping scans to be integrated and the point cloud to be enriched. In contrast, open trajectories suffer from spatial inhomogeneity and coverage gaps, resulting in lower density. To address this, approaches such as density modelling (Tan et al., 2025), sensor fusion (Tran et al., 2025) and trajectory optimization (Frías et al., 2022) have been proposed to enhance point cloud quality. However, some parameters such as DBH and fDBH were comparable or even slightly better in open trajectories. Open trajectories with RTK-GNSS SLAM enable reliable navigation, faster scanning, simpler planning and greater flexibility in complex terrain. Despite this, few studies have explicitly investigated open trajectories, e. g., a one line-transect PLS approach demonstrated accurate stand metrics (Ritter et al., 2024).

5. Conclusions

In summary the RTK-GNSS H-PLS showed the lowest noise and the most accurate stem parameters (DBH, ring thickness), while ZEB excelled in structural metrics such as tree height, vertical distribution, and crown, albeit with higher point cloud noise. BLK generally performed weakest due to its low scan rate and occasional outliers. Overall, scanner performance is primarily determined by point cloud completeness and canopy penetration. Parameters relying on lower stem geometry are robust across all systems, whereas metrics requiring detailed crown information are much more sensitive to occlusion, point density, and sensor limitations.

Additionally, it was demonstrated that the integration of RTK-GNSS into SLAM improves point cloud quality with respect to the derivation of tree parameters compared to SLAM without RTK-GNSS. The looped RTK-GNSS trajectory provided more consistent results than the open RTK-GNSS trajectory. However, the open trajectory also offers certain advantages. Therefore, different trajectory strategies without a loop closure and walking speed should be explored and tested to optimize point cloud quality and potentially increase point density.

At the same time, the accuracy of derived parameters strongly depends on segmentation quality and outlier filtering. Missing or incorrectly segmented tree parts can lead to wrong DBH, fDBH and tree position estimates. Fragmented tree segments therefore require reliable merging. Although the lower point density of the RTK-GNSS H-PLS does not strongly affect segmentation, improved filtering strategies are needed to preserve sparse crowns while maintaining robust filtering. The positional accuracy of RTK-GNSS H-PLS could be further validated using GCPs. Moreover, height estimation may be improved through data fusion with UAV or airborne LiDAR (Tran et al., 2025) or via semi-automatic treetop detection (Machado et al., 2025). Total, stem, and branch volume estimates can also benefit from fused drone and MLS point clouds, particularly under dense canopy conditions (Qi et al., 2022).

Acknowledgements

This work was funded by the project "Cross-border forest monitoring in the Bohemian Switzerland/Saxon Switzerland National Park" (TransForMon, 100736674) under the INTERREG Saxony–Czech Republic 2021–2027 programme, co-financed by the European Regional Development Fund (ERDF). The project runs from 20 May 2024 to 31 December 2027, with ERDF funding of 561,300.33€. We further thank the

Professorship of Photogrammetry, University of Applied Sciences Dresden, for providing the Leica BLK2GO, and Staatsbetrieb Sachsenforst for allowing data collection in Tharandt Forest.

Declaration of generative AI and AI-assisted technologies in the manuscript preparation process

During the preparation of this work the authors used You.com in order to assist with programming tasks and to improve the linguistic quality and readability. After using this tool/service, the authors reviewed and edited the content as needed and take full responsibility for the content of the published article.

References

Abegg, M., Boesch, R., Schaepman, M.E., Morsdorf, F., 2021. Impact of Beam Diameter and Scanning Approach on Point Cloud Quality of Terrestrial Laser Scanning in Forests. IEEE Transactions on Geoscience and Remote Sensing 59 (10), 8153–8167. https://doi.org/10.1109/TGRS.2020.3037763.

Cabo, C., Del Pozo, S., Rodríguez-Gonzálvez, P., Ordóñez, C., González-Aguilera, D., 2018. Comparing Terrestrial Laser Scanning (TLS) and Wearable Laser Scanning (WLS) for Individual Tree Modeling at Plot Level. Remote Sensing 10 (4), 540. https://doi.org/10.3390/rs10040540.

Chen, S., Liu, H., Feng, Z., Shen, C., Chen, P., 2019. Applicability of personal laser scanning in forestry inventory. PloS one 14 (2), e0211392. https://doi.org/10.1371/journal.pone.0211392.

Cho, H.-M., Park, J.-W., Lee, J.-S., Han, S.-K., 2024. Assessment of the GNSS-RTK for Application in Precision Forest Operations. Remote Sensing 16 (1), 148. https://doi.org/10.3390/rs16010148.

Chudá, J., Výbošťok, J., Tomaštík, J., Chudý, F., Tunák, D., Skladan, M., Tuček, J., Mokroš, M., 2024. Prompt Mapping Tree Positions with Handheld Mobile Scanners Based on SLAM Technology. Land 13 (1), 93. https://doi.org/10.3390/land13010093.

Feng, Q., Zhu, T., Ni, C., 2024. Forest point cloud denoising method based on curvature and density. International Journal of Remote Sensing 45 (22), 8105–8122. https://doi.org/10.1080/01431161.2024.2398228.

Frías, E., Previtali, M., Díaz-Vilariño, L., Scaioni, M., Lorenzo, H., 2022. Optimal scan planning for surveying large sites with static and mobile mapping systems. ISPRS Journal of Photogrammetry and Remote Sensing 192, 13–32. https://doi.org/10.1016/j.isprsjprs.2022.07.025.

Gollob, C., Ritter, T., Nothdurft, A., 2020. Forest Inventory with Long Range and High-Speed Personal Laser Scanning (PLS) and Simultaneous Localization and Mapping (SLAM) Technology. Remote Sensing 12 (9), 1509. https://doi.org/10.3390/rs12091509.

Henrich, J., van Delden, J., Seidel, D., Kneib, T., Ecker, A.S., 2024. TreeLearn: A deep learning method for segmenting individual trees from ground-based LiDAR forest point clouds. Ecological Informatics 84, 102888. https://doi.org/10.1016/j.ecoinf.2024.102888.

Hyyppä, E., Yu, X., Kaartinen, H., Hakala, T., Kukko, A., Vastaranta, M., Hyyppä, J., 2020. Comparison of Backpack, Handheld, Under-Canopy UAV, and Above-Canopy UAV Laser Scanning for Field Reference Data Collection in Boreal Forests. Remote Sensing 12 (20), 3327. https://doi.org/10.3390/rs12203327.

Kuželka, K., Marušák, R., Surový, P., 2022. Inventory of close-to-nature forest stands using terrestrial mobile laser scanning. International Journal of Applied Earth Observation and Geoinformation 115, 103104. https://doi.org/10.1016/j.jag.2022.103104.

Machado, M.D., Da Silva, G.F., Almeida, A.Q. de, Mendonça, A.R. de, Martins-Neto, R.P., Schimalski, M.B., 2025. Estimating Position, Diameter at Breast Height, and Total Height of Eucalyptus Trees Using Portable Laser Scanning. Remote Sensing 17 (16), 2904. https://doi.org/10.3390/rs17162904.

Muhojoki, J., Hakala, T., Kukko, A., Kaartinen, H., Hyyppä, J., 2024. Comparing positioning accuracy of mobile laser scanning systems under a forest canopy. Science of Remote Sensing 9, 100121. https://doi.org/10.1016/j.srs.2024.100121.

Pirti, A., Gümüş, K., Erkaya, H., Hoşbaş, R.G., 2010. Evaluating Repeatability of RTK GPS/GLONASS Near/Under Forest Environment. Croatian Journal of Forest Engineering : Journal for Theory and Application of Forestry Engineering 31 (1), 23–33. https://hrcak.srce.hr/file/86345.

Qi, Y., Coops, N.C., Daniels, L.D., Butson, C.R., 2022. Comparing tree attributes derived from quantitative structure models based on drone and mobile laser scanning point clouds across varying canopy cover conditions. ISPRS Journal of Photogrammetry and Remote Sensing 192, 49–65. https://doi.org/10.1016/j.isprsjprs.2022.07.021.

Qian, C., Liu, H., Tang, J., Chen, Y., Kaartinen, H., Kukko, A., Zhu, L., Liang, X., Chen, L., Hyyppä, J., 2017. An Integrated GNSS/INS/LiDAR-SLAM Positioning Method for Highly Accurate Forest Stem Mapping. Remote Sensing 9 (1), 3. https://doi.org/10.3390/rs9010003.

Raumonen, P., Åkerblom, M., 2022. TreeQSM. https://doi.org/10.5281/zenodo.6539580.

Ritter, T., Tockner, A., Krassnitzer, R., Witzmann, S., Gollob, C., Nothdurft, A., 2024. Optimizing line-plot size for personal laser scanning: modeling distance-dependent tree detection probability along transects. iForest - Biogeosciences and Forestry 17 (5), 269–276. https://doi.org/10.3832/ifor4588-017.

Shanghai Huace Navigation Technology Ltd., 2025. RS10. Handheld SLAM 3D Laser Scanner + GNSS RTK System.

Solares-Canal, A., Alonso, L., Picos, J., Armesto, J., 2023. Automatic tree detection and attribute characterization using portable terrestrial lidar. Trees 37 (3), 963–979. https://doi.org/10.1007/s00468-023-02399-0.

Soudarissanane, S., Lindenbergh, R., Menenti, M., Teunissen, P., 2011. Scanning geometry: Influencing factor on the quality of terrestrial laser scanning points. ISPRS Journal of Photogrammetry and Remote Sensing 66 (4), 389–399. https://doi.org/10.1016/j.isprsjprs.2011.01.005.

Tan, K., Zhang, S., Liu, S., 2025. Toward Point Cloud Density Consistency in Mobile Laser Scanning: A Mathematical Modeling and Correction Method. IEEE Geoscience and Remote Sensing Letters 22, 1–5. https://doi.org/10.1109/LGRS.2025.3580577.

Terryn, L., 2025. ITSMe: Individual Tree Structural Metrics. https://github.com/lmterryn/ITSMe.

Tran, L.T.N., Kim, M., Bang, H., Park, B.B., Choi, S.-M., 2025. Comparison of LiDAR Operation Methods for Forest Inventory in Korean Pine Forests. Forests 16 (4), 643. https://doi.org/10.3390/f16040643.

Tsintotas, K.A., Bampis, L., Gasteratos, A., 2022. The Revisiting Problem in Simultaneous Localization and Mapping: A Survey on Visual Loop Closure Detection. IEEE Transactions on Intelligent Transportation Systems 23 (11), 19929–19953. https://doi.org/10.1109/TITS.2022.3175656.

Vandendaele, B., Martin-Ducup, O., Fournier, R.A., Pelletier, G., Lejeune, P., 2022. Mobile Laser Scanning for Estimating Tree Structural Attributes in a Temperate Hardwood Forest. Remote Sensing 14 (18), 4522. https://doi.org/10.3390/rs14184522.

Winberg, O., Pyörälä, J., Yu, X., Kaartinen, H., Kukko, A., Holopainen, M., Holmgren, J., Lehtomäki, M., Hyyppä, J., 2023. Branch information extraction from Norway spruce using handheld laser scanning point clouds in Nordic forests. ISPRS Open Journal of Photogrammetry and Remote Sensing 9, 100040. https://doi.org/10.1016/j.ophoto.2023.100040.

Yang, J., Yuan, W., Lu, H., Liu, Y., Wang, Y., Sun, L., Li, S., Li, H., 2024. Assessing the Performance of Handheld Laser Scanning for Individual Tree Mapping in an Urban Area. Forests 15 (4), 575. https://doi.org/10.3390/f15040575.